



Response Surface Methodology for Photo Degradation of Methyl Orange Using Magnetic Nanocomposites Containing Zinc Oxide

Sedigheh Abbasi¹

Received: 3 March 2020 / Published online: 5 July 2020
© Springer Science+Business Media, LLC, part of Springer Nature 2020

Abstract

Magnetic graphen oxide ($\text{Fe}_3\text{O}_4\text{-GO}$) is applied for preparation of $\text{Fe}_3\text{O}_4\text{-GO-ZnO}$ (MGOZ) nanocomposite as photocatalyst. The photocatalysts are characterized by FTIR and UV spectrophotometer. FTIR results confirm the presence of Zn–O bonds and Fe–O bonds that are attributed to the ZnO and Fe_3O_4 , respectively. The removal efficiency of methyl orange (MO) is compared using MGOZ and $\text{Fe}_3\text{O}_4\text{-ZnO}$ at different irradiation time (ranging from 5 to 40 min) and pH (in the range of 3 to 11). The experimental results show that the removal efficiency of MO using MGOZ and $\text{Fe}_3\text{O}_4\text{-ZnO}$ enhanced with respect to the irradiation time. Meanwhile the lowest and highest removal efficiency are obtained at pH = 7 and pH = 3, respectively. The comparison between removal efficiency of MO using MGOZ and $\text{Fe}_3\text{O}_4\text{-ZnO}$ reveals that GO has a significant effect on the photocatalytic activity. Meanwhile, the removal efficiency of MO using MGOZ is higher than that of $\text{Fe}_3\text{O}_4\text{-ZnO}$. The statistical analysis of results using design of experiments (DOE) and Duncan's multiple range test at $\alpha = 0.05$ confirm that irradiation time, pH and their interactions have a significant effect on the removal efficiency of MO.

Keywords Magnetic graphen oxide · ZnO nanoparticles · Photo degradation · Design of experiments

Introduction

Graphene (Gr) as an allotrope of the carbon materials with two-dimensional structure has received abundant interests in the scientific investigations. Grapheme oxide (GO) as the most important derivative of Gr is extraordinary applied in the hybrid materials, composites and catalysts [1–4]. It may be attributed to the excellent specific surface area, hydrophilic property. The presence of the oxygen containing groups such as hydroxyl (OH) and carboxylic (COOH) in the structure of GO can eventuate to the conjunction between GO and different kinds of organic pollutants [5–7]. Therefore, the GO can be as an applicable material for augmentation of the adsorption capacity of organic pollutants that dissolved in the wastewater. Recently, the depletion of the industrial wastewater to the water sources such as seas and oceans is very detrimental

for the environment and can threaten the aquatic life [8–11]. Therefore, the elimination of the dispersed organic pollutants in the water systems is a critical issue. Among different decomposition procedures, photocatalytic oxidation of the organic pollutants is a common method that can be applied for a wide range of contaminants [7, 12–14]. The performance of the photocatalytic oxidation is dependent on the applied semiconductor and the amount of irradiated energy from the light source. Thus, irradiation of the dye organic suspension with energy higher than that of semiconductor's band gap can excite the electron from valence band to the conduction band of semiconductor. It leads to the formation of electron (e^-) and hole (h^+) in the conduction band and valence band, respectively. The produced electron–hole pairs are the most important factors in the production of reactive species in the decomposition of contaminants. The decomposition efficiency of the organic pollutants depends on the separation degree of the generated electric charges. [15–17]. The most-used single and hybrid semiconductors for purifying the organic pollutants are TiO_2 [9], SnO_2 [18, 19], ZnO [20], $\text{TiO}_2\text{-SnO}_2$ [9] and ZnO-SnO_2 [18, 19, 21].

✉ Sedigheh Abbasi
s.abbasi@esfarayen.ac.ir; abasi_1362@yahoo.com

¹ Central Research Laboratory, Esfarayen University of Technology, Esfarayen, North khorasan, Iran

The bonding of the semiconductors on the surface of materials with a high surface area (such as GO) can prevent the recombination of the produced electric charges and enhance the elimination of organic pollutants from wastewater. Based on the previous reported results, the attachment of different kinds of semiconductors on surface of GO leads to the enhancement of the removal efficiency of organic pollutants [22–24]. Due to the hydrophilic nature of GO, the separation of semiconductor-GO is very difficult and expensive. A practical way to overcome to this problem is the introducing of the magnetic nanoparticles such as Fe_3O_4 into the matrix of the applied semiconductors [25]. As a result, with the addition of an external field, semiconductors can be easily separated from the suspension. The decomposition of varying range of contaminants using $\text{ZnO-Fe}_2\text{O}_3$ [26] and $\text{Fe}_3\text{O}_4\text{-ZnO}$ [27–29] is studied by several researchers. Despite several studies for degradation of dye organic pollutants using GO-semiconductors and Fe_3O_4 -semiconductors, the application of Fe_3O_4 -GO-semiconductor is not yet been investigated. Therefore, in this study we want to synthesize the novel Fe_3O_4 -GO-ZnO nanocomposite for degradation of methyl orange as an organic dye pollutant. For this purpose, magnetic GO (MGO) is prepared by introducing the Fe_3O_4 nanoparticles on the surface of GO. Thus, the photocatalytic activity of the synthesized MGO-ZnO nanocomposites (MGOZ) is investigated for degradation of methyl orange (MO) as organic dye pollutant. The synthesized nanocomposites are characterized and the photocatalytic performance of them is optimized using design of experiments (DOE).

Experimental

Materials

Methyl orange (MO, $\text{C}_{14}\text{H}_{14}\text{N}_3\text{NaO}_3\text{S}$, 327.33 g/mol, 99.9%) as an organic dye pollutant is provided from Merck Company. The precursors of ZnO, SnO_2 and Fe_3O_4 are Zinc chloride (ZnCl_2) and Ferric acetylacetonate ($\text{Fe}(\text{acac})_3$), respectively. The other materials such as graphene oxide (GO), Ammonia solution (25%), Ammonium acetate (NH_4Ac) Ethylene glycol (EG) and Sodium hydroxide (NaOH) are the analytical grade.

Instruments

The Fourier transform infrared (FTIR) analysis is used for characterization of the functional groups on the surface of the synthesized samples. The characterization is done using a Tensor 70 and the percentage of the transmittance from each sample is recorded by variation of the wavenumber from 400 to 4000 cm^{-1} .

Preparation of MGO

The synthesis procedure of MGO is illustrated in Fig. 1. For a typical, the mixture of as received GO and EG (45 mg: 45 ml) is sonicated for about 30 min. Then, 0.225 g of $\text{Fe}(\text{acac})_3$ is dissolved in the prepared mixture and mixed 30 min using magnetic stirrer. Subsequently, 1.5 g NH_4Ac is dispersed in the above mixture. After 30 min agitation, the mixture is sealed in a Teflon autoclave and heated at $200\text{ }^\circ\text{C}$ for 24 h. The autoclave is cooled and prepared precipitated is separated from the solution using an external magnetic field. Finally, the collected precipitates are washed several times with distilled water and dried at $60\text{ }^\circ\text{C}$ for 24 h. The dispersing of the $\text{Fe}(\text{acac})_3$ leads to the preparation of Fe^{3+} in the suspension containing EG and GO. The released Fe^{3+} ions are captured using the oxygen containing groups such as hydroxyl and carboxyl. The applied NH_4Ac acts as a reducing agent of Fe^{3+} to Fe_3O_4 . In addition to the role of EG as a solvent, it can be considered as a reducing agent of GO and Fe^{3+} to grapheme Nano sheets and Fe_3O_4 , respectively.

Preparation of MGOZ

The precipitation method is applied for the preparation of MGOZ. At the first, 0.1 g of prepared MGO is added into distilled water (40 ml) and mixing is done using an ultrasound bath for about 30 min. Afterwards, 0.15 g of ZnCl_2 is added to the MGOZ suspension and the temperature of suspension is enhanced to $90\text{ }^\circ\text{C}$. Dispersion of ZnCl_2 leads to the formation of Zn^{2+} ions in the suspension. These produced ions is attached to the functional groups on the surface of GO and Fe_3O_4 .

After adding the aqueous solution of NaOH (5.3 ml, 5 M), Zn^{2+} ions are converted to the amorphous ZnO nanoparticles. Finally, the collected powders are washed and calcined at $300\text{ }^\circ\text{C}$ for about 3 h. The obtained sample is labeled as MGOZ#1.

The Photocatalytic Study

The Schematic of the photocatalytic experiments setup is presented in Fig. 2. Based on this Figure, it can be observed that a UV lamp (150 W) is placed in a quartz tube in the center of the photo reactor. The applied irradiation intensity is 13,000 Lumen. The temperature of the organic dye pollutant suspension containing synthesized photocatalysts is controlled using circulation of water. It can remove the heat generated by light source. Each experiment containing specified amount of prepared photocatalyst (ranging from 0.1 to 0.3%wt) is carried out in at different pH (3, 7 and 11). The photocatalytic performance

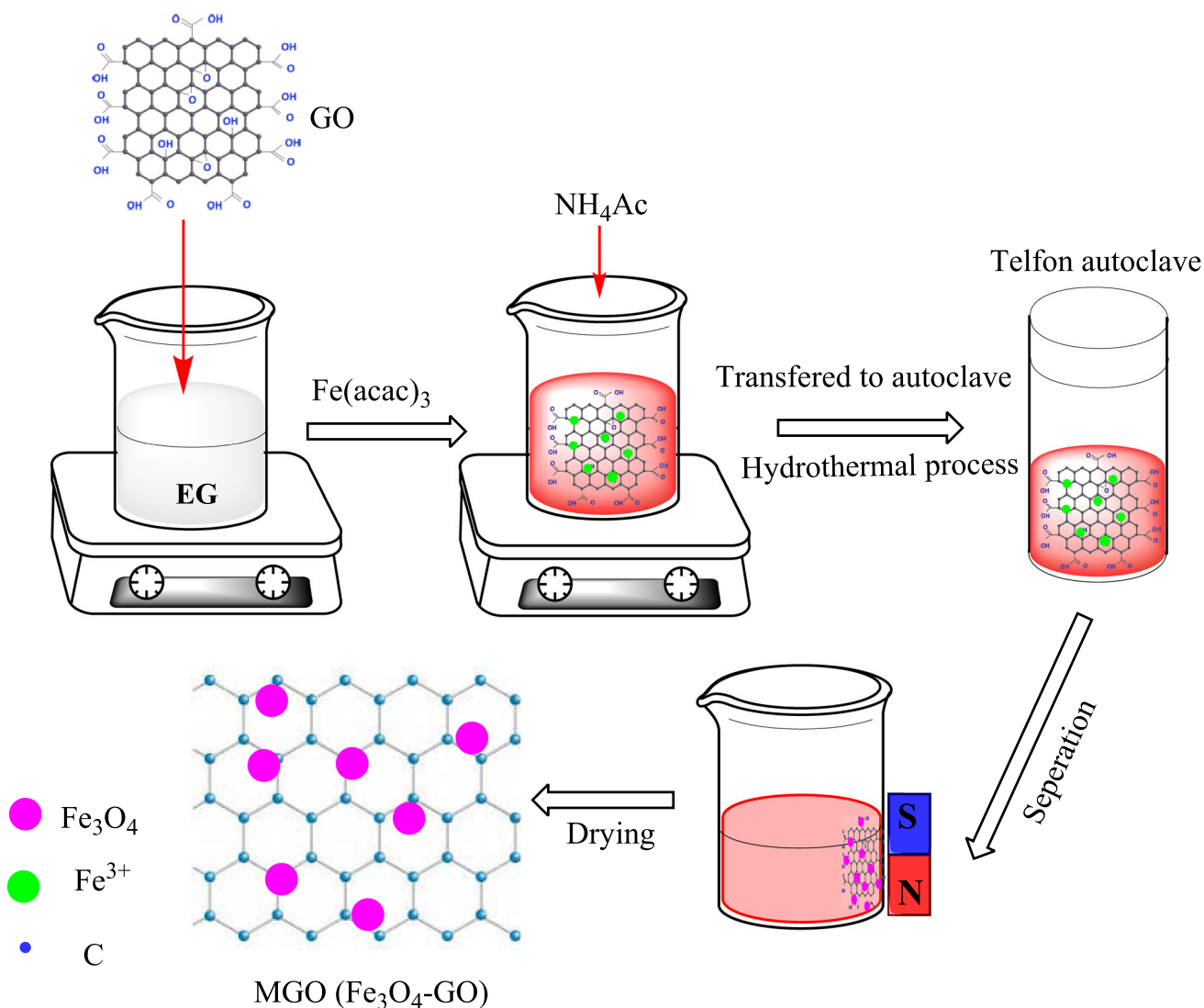


Fig. 1 Schematic of the synthesis procedure of MGO

of the synthesized photocatalysts is evaluated based on the photo degradation of MO (Eq. 1) [8, 9].

$$RE (\%) = \frac{A_0 - A_t}{A_0} \times 100. \tag{1}$$

where, RE is referred to the removal efficiency of MO, A₀ and A_t are the absorbance of MO solution (464 nm) at the beginning of the experiment without irradiation and time t with UV irradiation.

Statistical Analysis Study

Duncan’s multiple range test ($\alpha = 0.05$). is applied for investigation of the significance of the studied main parameters and the interaction between them. Meanwhile, according to this study the importance of the each level of the main factors can be specified. The statistical analysis

study is investigated using MSTAT-C software (Ver 1.42). Simultaneous analysis of more than one main parameter on the removal efficiency of MO is carried out using response surface methodology (RSM). For this purpose Minitab release software (ver 13.1) is applied.

Results and Discussion

FTIR Analysis

FT-IR spectroscopy is applied at room temperature to confirm the structure of the synthesized samples. According to the FTIR spectrum of MGO (Fig. 3), the peaks at 437 and 565 cm⁻¹ are assigned to E₂ mode of Zn-O bonds in ZnO [19] and the stretching vibration mode of Fe-O bonds in Fe₃O₄ [30], respectively. Additional peaks

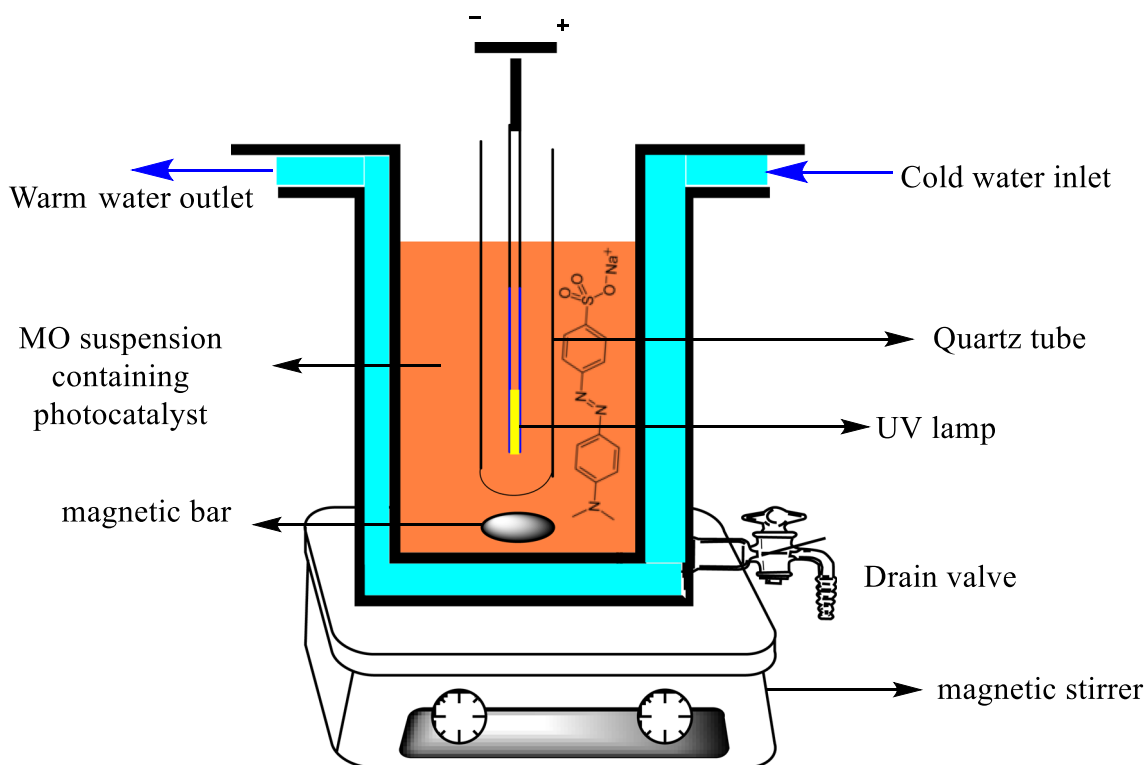


Fig. 2 Schematic of the photocatalytic experiments setup

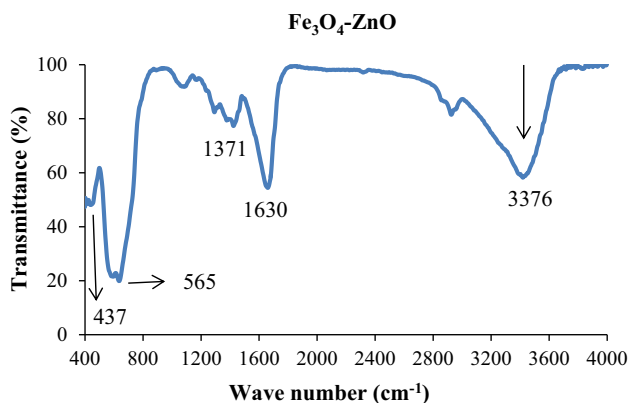


Fig. 3 FTIR spectra $\text{Fe}_3\text{O}_4\text{-ZnO}$

centered at 1371 and 1630 cm^{-1} may be due to the symmetrical and asymmetrical stretching of the zinc carboxylate [20, 31]. The appeared a broad peak at about 3376 cm^{-1} can be attributed to hydroxyl groups (O-H) [32–34]. The FTIR spectra MGOZ is presented in Fig. 4. As can be seen, a broad peak at about 3403 cm^{-1} may be assigned to the stretching vibrations of hydroxyl groups. Two main peaks centered at 440 and 568 cm^{-1} is attributed to the Zn–O bonds and Fe–O bonds, respectively. In addition, of the mentioned peaks, several peaks can be observed at 1076, 1160, 1550 and 1603 cm^{-1} that can be related to the alkoxy functional groups (C–O stretching),

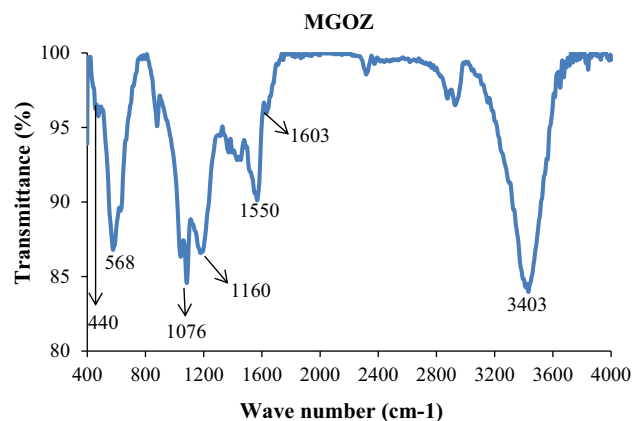


Fig. 4 FTIR spectra MGOZ

O–H deformation, =CH₂ groups and sp²-hybridized C=C [31, 35], respectively.

Interaction Analysis Among Main Factors

Figures 5 and 6 illustrate the interaction between irradiation time and pH (A–B) for removal efficiency of MO using $\text{Fe}_3\text{O}_4\text{-ZnO}$ and MGOZ, respectively. The results of these Figures confirm that the curves of the removal efficiency variations at different irradiation time are not parallel to each other. It means that both of the main factors (irradiation time and pH) have the significant influence on

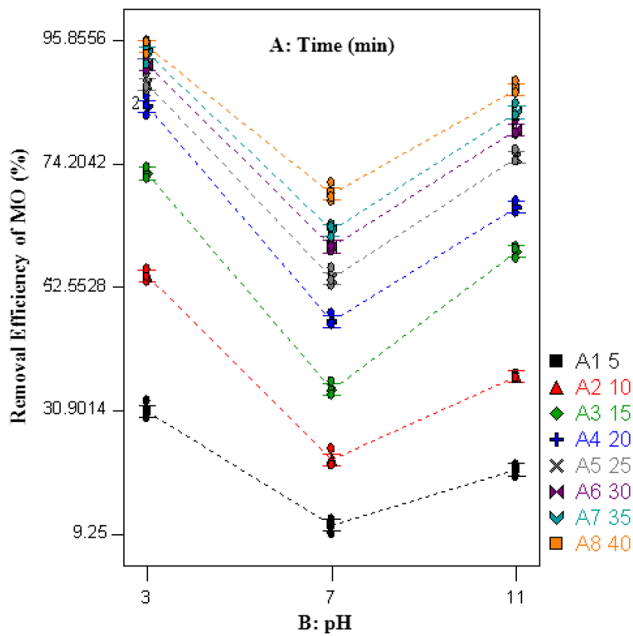


Fig. 5 Interaction between irradiation time and pH (A–B) for removal efficiency of MO using Fe₃O₄-ZnO

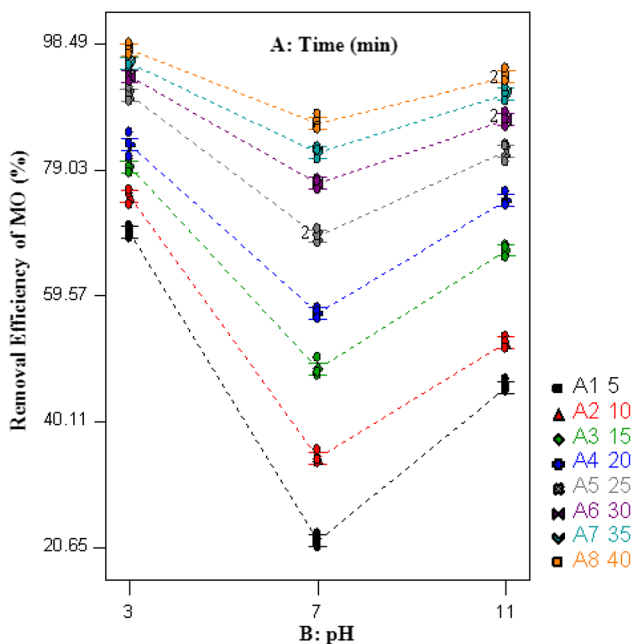


Fig. 6 Interaction between irradiation time and pH (A–B) for removal efficiency of MO using MGOZ

each other. Therefore, the interaction between main factors can be considered as a significant parameter in the modeling of removal efficiency variation with respect to the main factors and their interactions [16]. Meanwhile, the results of Figs. 5 and 6 reveal that the removal efficiency of MO using both of the synthesized nanocomposites enhance with respect to the irradiation time. It may be attributed to

the influence of UV light energy on the stimulation of electron and transmission from valence band to the conduction band [36–38]. Therefore, increasing the irradiation time (from 5 min to 40 min) to the suspension containing organic dye pollutant and photocatalysts leads to the enhancement of electron excitation. To the number of excited electrons, the electron (e^-) and hole (h^+) can be produced in the conduction band and valence band, respectively. The produced e^-h^+ pairs can adsorb the soluble oxygen in the suspension and water, respectively. It can lead to the generation of oxidant radicals such as O_2^- and OH^\cdot [13, 20, 36]. Thus, the amount of produced oxidant radicals and removal efficiency of MO enhance by increasing the irradiation time. Based on the variation of removal efficiency of MO with respect to pH, it can be seen that the lowest and highest removal efficiency of MO using Fe₃O₄-ZnO and MGOZ occur at pH = 7 and pH = 3, respectively. The high removal efficiency of MO at pH = 3 is due to the presence of a large amount of hydrogen ions (H^+) in the suspension. The hydrogen ions in the suspension are capable of absorbing soluble oxygen. The reaction between hydrogen ions and oxygen leads to the formation of active radicals such as OH^\cdot . Consequently, the formed ions can decompose the organic pollutants [37, 39]. Hence, the photocatalytic activity of the applied photocatalysts can be enhanced in the acidic suspensions. As well due to the presence of the charge on the surface of the synthesized photocatalysts, the dispersibility of them in the solution increases dramatically [13, 40]. Therefore, it can be eventuate to the enhancement of active surface area, excitation of electrons in the valence band and photo degradation of MO.

Analysis the Studied Levels of Main Factors

The effect of each level of main factors on the removal efficiency of MO is investigated based on Duncan's

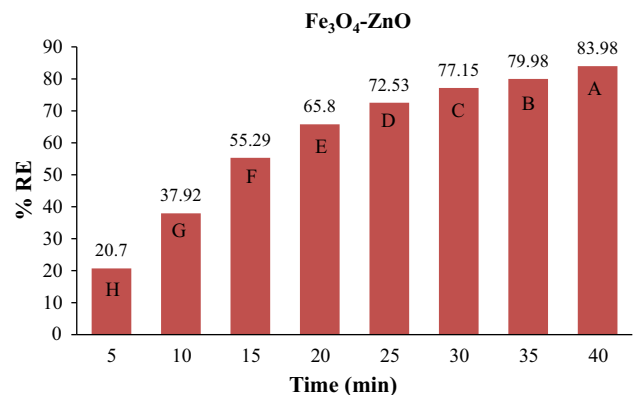


Fig. 7 The alteration of removal efficiency of MO using Fe₃O₄-ZnO with respect to irradiation time

multiple range test at 95% level of probability ($\alpha = 0.05$). Figures 7 and 8 illustrate the influence of irradiation time on the removal efficiency of MO using $\text{Fe}_3\text{O}_4\text{-ZnO}$ and MGOZ, respectively. As can be seen, the removal efficiency of MO using $\text{Fe}_3\text{O}_4\text{-ZnO}$ and MGOZ increases by enhancement irradiation time from 5 to 40 min. The observed enhancement can be attributed to the effect of irradiation time on the transition of excited electrons from valence band to the conduction band [19, 20]. Meanwhile, the results of Figs. 7 and 8 confirm that there is a significant difference among studied levels of irradiation time at $\alpha = 0.05$. The maximum removal efficiency of MO using both of the synthesized photocatalysts is happens at 40 min. The values of the removal efficiency of MO using $\text{Fe}_3\text{O}_4\text{-ZnO}$ and MGOZ at 40 min of irradiation time are 83.98% and 92.34%, respectively. It is clear that the removal efficiency of MO using MGOZ is higher than that of $\text{Fe}_3\text{O}_4\text{-ZnO}$. It can be related to the effect of GO. The introducing of GO in the $\text{Fe}_3\text{O}_4\text{-ZnO}$ structure can decrease the recombination rate of produced e^-h^+ pairs. Meanwhile, a large amount of organic dye pollutant can attach to the surface of MGOZ base on π - π stacking due to the aromatic nature of GO [41].

Figures 9 and 10 show the alteration of removal efficiency of MO with respect to pH using $\text{Fe}_3\text{O}_4\text{-ZnO}$ and MGOZ, respectively. Based on these two Figures, it can be deduced that all three pH (pH = 3, pH = 7 and pH = 11) have significant effect on the removal efficiency. The comparison between removal efficiency of MO using both of applied photocatalysts reveals that at each studied pH the photocatalytic activity of MGOZ is higher than that $\text{Fe}_3\text{O}_4\text{-ZnO}$. As mentioned above, it can be due to the presence of GO in the MGOZ nanocomposite. Also, the results show that the highest removal efficiency using both of used photocatalysts are at pH = 3. The obtained results are in agreement with previous reports [37, 39, 42].

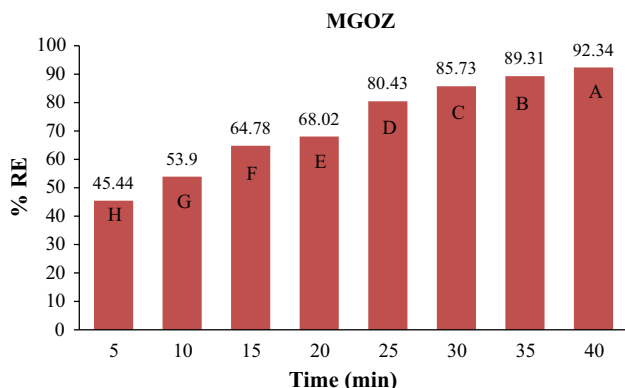


Fig. 8 The alteration of removal efficiency of MO using MGOZ with respect to irradiation time

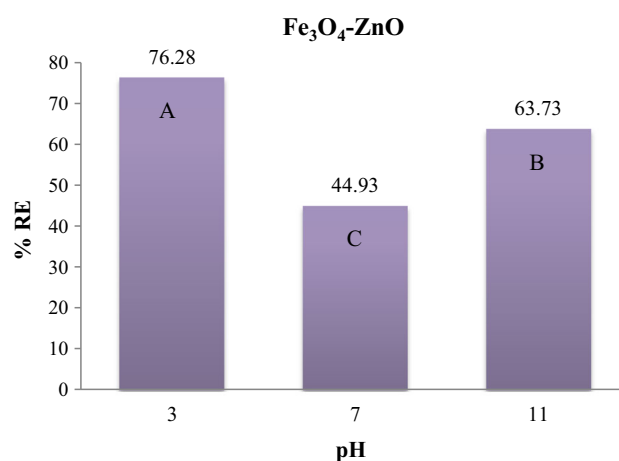


Fig. 9 The alteration of removal efficiency of MO using $\text{Fe}_3\text{O}_4\text{-ZnO}$ with respect to pH

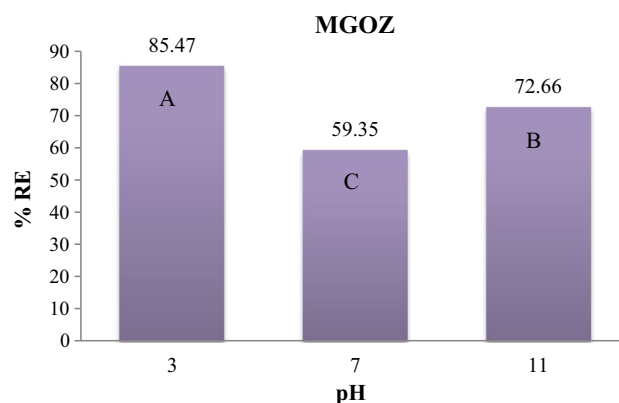


Fig. 10 The alteration of removal efficiency of MO using MGOZ with respect to pH

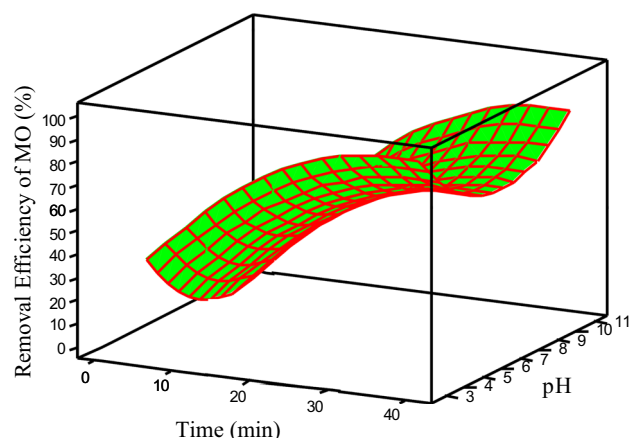


Fig. 11 Response surface of the removal efficiency of MO using $\text{Fe}_3\text{O}_4\text{-ZnO}$

Response Surface Analysis

Response surface of the removal efficiency of MO using $\text{Fe}_3\text{O}_4\text{-ZnO}$ and MGOZ are presented in Figs. 11 and 12, respectively. The results of these Figures confirm that the photocatalytic activity of the both samples enhances by increasing the irradiation time. Although, the variation of the removal efficiency of MO using $\text{Fe}_3\text{O}_4\text{-ZnO}$ is lower than that of MGOZ. It can be attributed to the recombination rate of produced electron-hole pairs. In fact, the recombination rate in the synthesized MGOZ is lower than that of $\text{Fe}_3\text{O}_4\text{-ZnO}$. Therefore, the sequence of the photocatalytic activity is $\text{Fe}_3\text{O}_4\text{-ZnO} < \text{MGOZ}$. According to the variation of removal efficiency with respect to the pH, it is clear that the minimum photo degradation of MO is observed at $\text{pH} = 7$. So that increasing pH from 3 to 7 leads to the decreasing the photocatalytic activity of both samples. It is due to the reduction of hydrogen ions (H^+) in the suspension [13, 36]. Then the enhancement of pH from 7 to 11 eventuates to the increment of removal efficiency. Meanwhile, it can be confirm that the dependence of the removal efficiency to irradiation time is more than pH. In fact, the amount of produced reactive radicals enhance with respect to irradiation time.

The contour lines of the removal efficiency of MO using $\text{Fe}_3\text{O}_4\text{-ZnO}$ and MGOZ are presented in Figs. 13 and 14. The dependence of irradiation time to applied pH can be observed from these contour lines. It is clear that for obtain the desired value of removal efficiency, the irradiation time enhances by augmentation of pH from 3 to 7. Subsequently, by increasing pH of suspension ranging from 7 to 11, required irradiation time decreases. Therefore, based on contour lines, the optimum values of main parameter such as irradiation time and pH can be calculated.

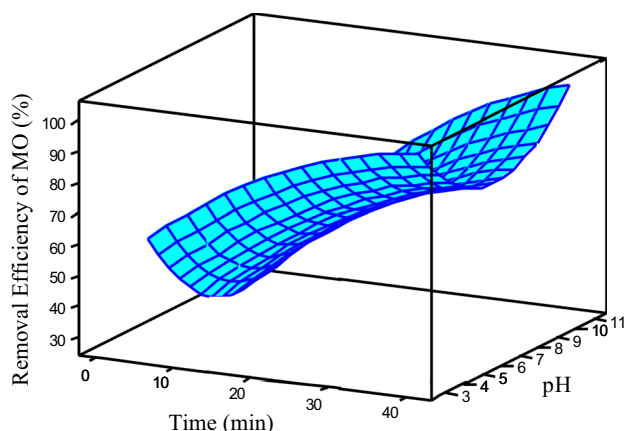


Fig. 12 Response surface of the removal efficiency of MO using MGOZ

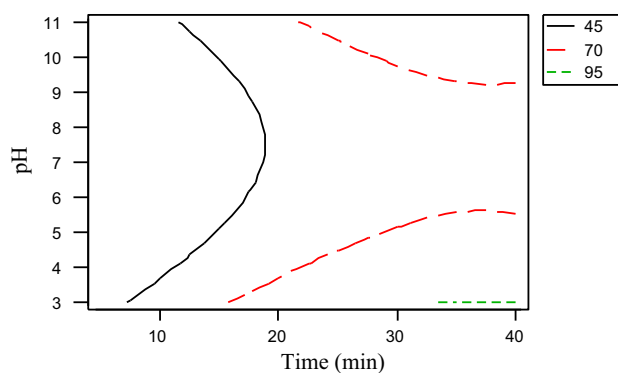


Fig. 13 The dependence of the removal efficiency of MO using $\text{Fe}_3\text{O}_4\text{-ZnO}$ to irradiation time and pH based on contour lines

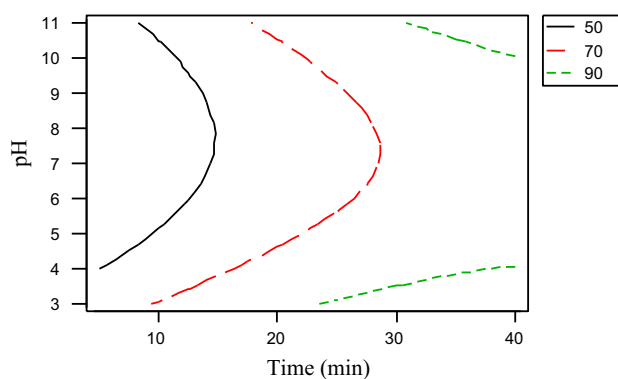


Fig. 14 The dependence of the removal efficiency of MO using MGOZ to irradiation time and pH based on contour lines

Conclusions

In this study, we present the preparation and characterization of $\text{Fe}_3\text{O}_4\text{-ZnO}$ and MGOZ nanocomposites as photocatalyst for degradation of MO. The photocatalytic activity study reveals that the removal efficiency of MO increases by enhancement of irradiation time. Meanwhile the results show that the variation of the removal efficiency with pH is not linear. The results of Duncan's multiple range test show that all studied levels of irradiation time (5, 10, 15, 20, 25, 30, 35 and 40 min) and pH (3, 7 and 11) have a significant effect on the removal efficiency at 95% level of probability. The sequence of the photocatalytic activity is $\text{Fe}_3\text{O}_4\text{-ZnO} < \text{MGOZ}$.

Acknowledgements The authors of this study thank the head of the Central Research Nano Laboratory of Esfarayen University of Technology for the license to use the equipment.

Compliance with Ethical Standards

Conflict of interest We declare that we have no financial and personal relationships with other people or organisation that can inappropriately influence our work.

References

- L. Gan, H. Li, L. Chen, L. Xu, J. Liu, A. Geng, et al. (2018). *Colloid Polym. Sci.* **296**, (3), 607–615.
- Y.-C. Chen, K.-I. Katsumata, Y.-H. Chiu, K. Okada, N. Matsushita, and Y.-J. Hsu (2015). *Appl. Catal. A General.* **490**, 1–9.
- Y.-C. Pu, H.-Y. Chou, W.-S. Kuo, K.-H. Wei, and Y.-J. Hsu (2017). *Appl. Catal. B Environ.* **204**, 21–32.
- Y.-S. Chang, P.-Y. Hsieh, T.-F. M. Chang, C.-Y. Chen, M. Sone, and Y.-J. Hsu (2020). *J. Mater. Chem. A.* <https://doi.org/10.1039/d0ta02359k>.
- R. Kumar, R. K. Singh, D. P. Singh, R. Savu, and S. A. Moshkalev (2016). *Mater. Design.* **111**, 291–300.
- K.-A. Tsai and Y.-J. Hsu (2015). *Appl. Catal. B Environ.* **164**, 271–278.
- K.-A. Tsai, P.-Y. Hsieh, T.-H. Lai, C.-W. Tsao, H. Pan, Y.-G. Lin, et al. (2020). *ACS Appl. Energy Mater.* **3**, 5322–5332.
- S. Abbasi (2016). *Iran. J. Health Environ.* **9**, (3), 433–442.
- S. Abbasi (2018). *Mater. Res. Express.* **5**, 066302.
- S. Abbasi (2020). *J. Inorgan. Organometal. Polym. Mater.* **30**, 1924–1934.
- S. Abbasi, F. Ahmadpoor, M. Imani, and M.-S. Ekrami-Kakhki (2020). *Int. J. Environ. Anal. Chem.* **100**, (2), 225–240.
- S. Abbasi, M.-S. Ekrami-Kakhki, and M. Tahari (2017). *J. Mater. Sci. Mater. Electron.* **28**, (20), 15306–15312.
- S. Abbasi and M. Hasanpour (2017). *J. Mater. Sci. Mater. Electron.* **28**, (2), 1307–1314.
- Y.-H. Chiu, T.-F. M. Chang, C.-Y. Chen, M. Sone, and Y.-J. Hsu (2019). *Catalysts* **9**, 430.
- N. Roozban, S. Abbasi, and M. Ghazizadeh (2017). *J. Mater. Sci. Mater. Electron.* **28**, (8), 6047–6055. <https://doi.org/10.1007/s10854-016-6280-9>.
- S. Abbasi, M. Hasanpour, and M. S. E. Kakhki (2017). *J. Mater. Sci. Mater. Electron.* **28**, (13), 9900–9910. <https://doi.org/10.1007/s10854-017-6745-5>.
- Y.-H. Chiu, T.-H. Lai, M.-Y. Kuo, P.-Y. Hsieh, and Y.-J. Hsu (2019). *Appl. Mater.* **7**, 080901.
- A. Ghaderi, S. Abbasi, and F. Farahbod (2015). *Iran. J. Chem. Eng.* **12**, (3), 96–105.
- A. Ghaderi, S. Abbasi, and F. Farahbod (2018). *Mater. Res. Express.* **5**, 065908.
- N. Roozban, S. Abbasi, and M. Ghazizadeh (2017). *J. Mater. Sci. Mater. Electron.* **28**, (10), 7343–7352. <https://doi.org/10.1007/s10854-017-6421-9>.
- W. W. Wang, Y. J. Zhu, and L. X. Yang (2007). *Adv. Funct. Mater.* **17**, 59–64.
- A. Sanmugam, D. Vikraman, H. J. Park, and A. H.-S. Kim (2017). *Nanomaterials* **7**, 363–376.
- M. Azarang, A. Shuhaimi, R. Yousefi, A. M. Golsheikh, and M. Sookhakian (2014). *Ceramics Int.* **40**, 10217–10221.
- M. Azarang, A. Shuhaimi, and M. Sookhakian (2015). *RSC Adv.* **5**, 53117–53128.
- S. Kurinobu, K. Tsurusaki, Y. Natui, M. Kimata, and M. Hasegawa (2007). *J. Magn. Magn. Mater.* **310**, e1025–e1027.
- D. Li, H. Haneda, and J. Photochem (2003). *J. Photochem. Photobiol. A.* **160**, (3), 203–212.
- M. Nikazar, M. Alizadeh, R. Lalavi, and M. H. Rostami (2014). *Iran. J. Environ. Health Sci. Eng.* **12**, 21–26.
- M. Safari, M. H. Rostami, M. Alizadeh, A. Alizadehbirjandi, S. A. A. Nakhli, and R. Aminzadeh (2014). *J. Environ. Health Sci. Eng.* **12**, (1), 1–10.
- D. S. Winatapura, S. H. Dewi, and W. A. Adi (2016). *Int. J. Technol.* **3**, 408–416.
- M. Abareshi, E. K. Goharshadi, S. M. Zebbarjad, H. K. Fadafan, and A. Youssefi (2010). *J. Magn. Magn. Mater.* **322**, 3895–3901.
- A. K. Zak, W. H. A. Majid, M. Darroudi, and R. Yousefi (2011). *Mater. Lett.* **65**, 70–73.
- S. Abbasi, S. M. Zebbarjad, S. H. N. Baghban, and A. Youssefi (2015). *Synth. React. Inorgan. Metal Organ. Nano Metal Chem.* **45**, 1539–1548.
- D. Dastan, N. Chaure, and M. Kartha (2017). *J. Mater. Sci. Mater. Electron.* **28**, 7784–7796.
- D. Dastan, S. L. Panahi, and N. B. Chaure (2016). *J. Mater. Sci. Mater. Electron.* **27**, 12291–12296.
- A. Akbarzadeh, M. Samiei, S. W. Joo, M. Anzaby, Y. Hanifehpour, H. T. Nasrabadi, et al. (2012). *J. Nanobiotechnol.* **10**, 46–58.
- S. Abbasi (2019). *Environ. Monitor. Assess.* **191**, (4), 206–218.
- S. Abbasi and M. Hasanpour (2017). *J. Mater. Sci. Mater. Electron.* **28**, (16), 11846–11855. <https://doi.org/10.1007/s10854-017-6992-5>.
- S. Abbasi, M. Hasanpour, F. Ahmadpoor, M. Sillanpää, D. Dastan, and A. Achour (2020). *Int. J. Environ. Anal. Chem.* <https://doi.org/10.1080/03067319.2019.1662414>.
- S. H. Borji, S. Nasserri, R. Nabizadeh, A. H. Mahvi, and A. H. Javadi (2011). *Iran. J. Health Environ.* **3**, (4), 369–380.
- H. Yuan and J. Xu (2010). *Int. J. Chem. Eng. Appl.* **1**, (3), 214–246.
- S. P. Kim, M. Y. Choi, and H. C. Choi (2015). *Appl. Surf. Sci.* **357**, 302–308.
- K. Byrappa, A. S. Dayananda, C. P. Sajan, B. Basavalingu, M. B. Shayan, K. Soga, et al. (2008). *J Mater Sci.* **43**, 2348–2355.

Publisher's Note Springer Nature remains neutral with regard to jurisdictional claims in published maps and institutional affiliations.